Cancer immunotherapy responses persist after lymph node resection

Hengbo Zhou[1,2], James W. Baish[3], Meghan J. O'Melia[1], Laurel B. Darragh[4], Emma Specht[5], Juliane Czapla[5], Pin-ji Lei[1], Lutz Menzel[1], Johanna J. Rajotte[1], Mohammad R. Nikmaneshi[1], Mohammad S. Razavi[1], Matthew G. Vander Heiden[2,6], Jessalyn M. Ubellacker[7], Lance L. Munn[1], Genevieve M. Boland[5], Sonia Cohen[5], Sana D. Karam[4] and Timothy P. Padera[1]

1. Edwin Steele Laboratories, Department of Radiation Oncology, Massachusetts General Hospital

2. Koch Institute for Cancer Research and Department of Biology, Massachusetts Institute of Technology

3. Department of Biomedical Engineering, Bucknell University

4. Department of Radiation Oncology, University of Colorado Anschutz Medical Campus

5. Department of Surgery, Massachusetts General Hospital

6. Department of Medical Oncology, Dana-Farber Cancer Institute

7. Department of Molecular Metabolism, Harvard T.H. Chan School of Public Health

ABSTRACT:

Surgical removal of lymph nodes (LNs) to prevent metastatic recurrence, including sentinel lymph node biopsy (SLNB) and completion lymph node dissection (CLND), are performed in routine practice. However, it remains controversial whether removing LNs which are critical for adaptive immune responses impairs immune checkpoint blockade (ICB) efficacy. Here, our retrospective analysis demonstrated that stage III melanoma patients retain robust response to anti-PD1 inhibition after CLND. Using orthotopic murine mammary carcinoma and melanoma models, we show that responses to ICB persist in mice after TDLN resection. Mechanistically, after TDLN resection, antigen can be re-directed to distant LNs, which extends the

responsiveness to ICB. Strikingly, by evaluating head and neck cancer patients treated by neoadjuvant durvalumab and irradiation, we show that distant LNs (metastases-free) remain reactive in ICB responders after tumor and disease-related LN resection, hence, persistent anti-cancer immune reactions in distant LNs. Additionally, after TDLN dissection in murine models, ICB delivered to distant LNs generated greater survival benefit, compared to systemic administration. In complete responders, anti-tumor immune memory induced by ICB was systemic rather than confined within lymphoid organs. Based on these findings, we constructed a computational model to predict free antigen trafficking in patients that will undergo LN dissection.

INTRODUCTION:

Recent advances in understanding of the mechanisms of T cell activation and exhaustion led to the identification of several immune checkpoints, such as programmed death 1 (PD-1)(1, 2) and cytotoxic T lymphocytes antigen 4 (CTLA-4)(3, 4), which have been used as therapeutic targets(5, 6). Immune checkpoint blockade (ICB) has been approved to treat many cancers including melanoma(7, 8), non-small cell lung cancer(9, 10), renal cell carcinoma(11), Hodgkin lymphoma(12), hepatocellular carcinoma(13, 14), and gastric carcinoma(15). However, an improved understanding of ICB mechanisms *in vivo* is necessary for immunotherapy to benefit more patients.

Lymph nodes (LNs) are secondary lymphoid organs that surveil tissue fluids and initiate adaptive immunity(16). Due to the direct drainage of interstitial fluid from tumor tissue in the lymphatic basin (lymphosome), metastatic dissemination to tumor-draining lymph nodes (TDLNs) occurs in the early stage of cancer growth(17). Colonization in LNs can block nodal

46 entry of naïve lymphocytes(18), expand regulatory T cells (Tregs)(19, 20) and induce systemic
47 tolerance to favor distant metastasis of cancer cells(20). LN metastases can also further
48 disseminate to additional metastatic sites(21, 22). Therefore, LN metastatic burden is a strong
49 prognostic factor for patient outcome. Sentinel lymph node biopsy (SLNB) and completion
50 lymph node dissection (CLND) are commonly performed(23-27) to help stage disease and
51 reduce disease burden.

52 Seminal work has demonstrated that tumor-specific T cells and non-exhausted tumor-specific
53 memory cells are enriched in TDLNs, but not in non-TDLNs(28, 29). In addition, PD-1/PD-L1
54 interaction between conventional dendritic cells (DCs) (PD-L1+) and tumor-specific T cells (PD-
55 1+) is abundant in TDLNs(28). Intrapleural delivery of low-dose PD-L1 antibody to TDLNs can
56 induce anti-tumor immunity against AC29 tumors (mesothelioma)(28). Additional studies, using
57 B16F10 (melanoma), 4T1 (mammary carcinoma) and E0771(mammary carcinoma) tumors,
58 found selective administration of ICB to TDLNs can improve ICB potency, compared to
59 systemic administration(30, 31). These data suggest that removal of TDLNs could potentially
60 impair ICB outcome. Indeed, anti-PD-1 or anti-4-1BB efficacy can be abolished by TDLN
61 dissection in MC38 (colon adenocarcinoma) or CT26 (colon carcinoma) tumors ectopically
62 grafted in the skin(32, 33). Similarly, responses can be ablated by TDLN lymphadenectomy at
63 any point during anti-PD-L1 treatment in subcutaneously grafted B16F10 (melanoma) tumors
64 expressing lymphocytic choriomeningitis virus glycoprotein(29). However, in the phase III
65 clinical trial NCT00636168, completely resected stage III melanoma patients, from whom
66 sentinel LNs and metastatic LNs were removed, still responded and benefited from ipilimumab
67 (targeting CTLA-4), indicating that persistent presence of TDLNs may not be required for ICB
68 efficacy(34). Further, in the phase I trial NCT04274816, lymphatic basin administration of

69 tremelimumab (targeting CTLA4) after tumor resection led to a systemic reduction of Tregs and
70 activation of effector T cells. This response persisted up to 3 months after subsequent SLNB,
71 suggesting that the ICB-mediated immune response was not confined only within sentinel
72 LNs(35). Due to the important role of LNs in the adaptive immune response, it is imperative to
73 evaluate the effects of SLNB and CLND on ICB efficacy.

74 Here, through retrospective analysis, we found that regardless of the extent of LN surgery, stage
75 III melanoma patients—surprisingly even those with CLND—benefited from adjuvant anti-PD1
76 inhibition. By using orthotopic breast cancer and melanoma models in mice, we demonstrate that
77 ICB efficacy persists after TDLN dissection. Mechanistically, after TDLN dissection, antigen
78 can be transported to distant LNs through redirected lymph drainage, which contributes to the
79 residual responsiveness to ICB. This phenomenon is corroborated in head and neck cancer
80 patients—treated by neoadjuvant durvalumab and irradiation therapy followed by adjuvant
81 durvalumab—by the presence of reactive distant LNs after primary tumor resection and LN
82 dissection. Finally, compared to systemic administration, ICB delivered to reactive distant LNs
83 generates greater response after TDLN dissection.

84 RESULTS:

85 Stage III melanoma patients respond to ICB after CLND

86 Prior to the availability of effective systemic therapies for patients with melanoma, LN surgery
87 played a major role in the treatment of patients with locoregional disease. Any patient with
88 clinically evident LN metastases or a positive SLNB underwent CLND for disease control. In
89 2017 MSLT-II(36), a randomized trial of CLND vs observation in patients with positive SLNB,
90 demonstrated that CLND provided no melanoma-specific survival (MSS) benefit to patients with

91 melanoma identified within the SLN. Given the morbidity of CLND, this trial changed clinical
92 practice to favor observation after a positive SLNB, with CLND reserved for clinical disease
93 recurrence in the draining LN basin. Approximately 20% of patients would ultimately recur in
94 the draining nodal basin, sparing 80% of patients with a positive SLNB from the unnecessary
95 morbidity of CLND(36).

96 With the approval of effective systemic therapies, the role of LN surgery—other than for
97 staging—has been called into question. Given the importance of TDLNs for ICB response in
98 mouse models(29, 32, 33), we asked whether the extent of LN surgery would impact the
99 effectiveness of ICB treatment. To assess this, we analyzed a cohort of 66 patients who
100 underwent surgery for stage III melanoma followed by adjuvant treatment with at least one line
101 of anti-PD1 therapy (nivolumab or pembrolizumab) at Massachusetts General Hospital. Within
102 this adjuvant ICB cohort, 50 patients underwent SLNB alone while 16 patients underwent
103 CLND. Surprisingly, there was no statistically significant difference in MSS (**Figure 1 A**) or
104 recurrence-free survival (RFS) (**Figure 1 B**) between patients who underwent SLNB alone
105 versus those who underwent CLND. After further stratification, no difference was detected in
106 local (**Figure 1 C**) or distant (**Figure 1 D**) RFS either. These data demonstrate that response to
107 ICB persists in patients who have undergone CLND surgery, and that the extent of LN surgery
108 within the draining lymph node basin does not impact outcomes in the setting of ICB.

109 **ICB response persists after TDLN dissection in mice**

110 To experimentally test the impact of TDLN dissection on ICB efficacy in murine models, we
111 used orthotopic, syngeneic mouse melanoma (B16F10) and mammary carcinoma (E0771)
112 models. At first, we evaluated the metastatic status of TDLNs following timeline described in

113 recent studies (29, 32). After three doses of IgG or anti-PD1 treatment (starting from day 7 every
114 other day and ending on day 13 since tumor implantation), incidence of micro-metastases in LNs
115 was detected, especially, in IgG-treated mice (Supp **Figure 1A**). For LN surgery, SLNB was
116 modeled by removing the inguinal (IN) LN in C57BL6 mice, which drains the upper hindleg and
117 4th mammary fat pad of mice. Sham LN removal surgery was performed on all animals in control
118 groups. After 10 days of recovery, B16F10 or E0771 cells were introduced to the dermis on the
119 lower flank or 4th mammary fat pad, respectively. 7 days later, 3 doses of PD-1 blocking
120 antibody (10mg/kg) were administered intraperitoneally (every 2 days for B16F10 tumors or
121 every 3 days for E0771 tumors). Compared to IgG control treated mice, PD-1 inhibition
122 increased overall survival in both the sham and SLN removed (SLNB) mice. Interestingly, in
123 groups treated with anti-PD-1, there was no difference in overall survival between the sham
124 surgery mice and the SLNB counterparts (**Figure 2A**). To mimic CLND, a radical procedure that
125 is increasingly less common(36-39), ipsilateral IN, axillary (AX), and brachial (BR) LNs were
126 surgically removed, as each is in the region can receive lymphatic drainage from the tumor
127 site(33, 40). Similar to SLNB, response to PD-1 inhibition persists after CLND (**Figure 2B**).

128 Next, we measured whether anti-tumor immunity is retained solely in TDLNs after tumor
129 establishment. Thus, we tested the effects of SLNB and CLND after primary tumor implantation.
130 B16F10 or E0771 cells were orthotopically implanted 6 days prior to surgery. Sham, SLNB or
131 CLND was performed at day 6 and 3 doses of anti-PD-1 treatment was initiated at day 7 (every 2
132 days for B16F10 tumors or every 3 days for E0771 tumors). Similar to pre-emptive surgery,
133 response to PD-1 inhibition persists after SLNB or CLND (**Figure 2C**). Although there was no
134 significant decrease in survival after LN surgery, fewer mice remained tumor-free in the LN
135 dissection conditions (**Figure 2D)**. These findings are not consistent with recent investigations

136 using MC38 and CT26 tumor models grown ectopically in the subcutaneous setting(32, 33). To
137 determine whether implantation site can affect ICB outcome, E0771 cells were introduced to the
138 dermis and LN dissection was conducted either pre-emptively or after tumor establishment.
139 Intriguingly, aggressive CLND impaired anti-PD-1 efficacy in the ectopic setting (**Supp Figure**
140 **1 B&C**), indicating altered immune response can occur when tumor cells are introduced to an
141 ectopic site.

142 **Remaining LNs are required for ICB response after TDLN dissection**

143 Because of the surprising finding that benefit of ICB treatment persists in mice after LN
144 resection, we sought to examine whether LNs in general are essential for ICB response. To that
145 end, lymphotoxin alpha (Lta) knock out (KO) mice —*Lta*^{tm1Dch} (C57bl/6 background), referred to
146 throughout as *Lta* KO mice were used. These mice lack Peyer's patches and multiple LNs
147 including popliteal (PO), IN, BR and AX LNs, among other missing lymphoid tissues(41).
148 Although the splenic structure is disorganized by *Lta* deletion, the number of lymphocytes, the
149 composition of the types of lymphocytes and their homing and effector abilities are normal in
150 both the spleen and in peripheral blood(41-44). B16F10 or E0771 cells were orthotopically
151 implanted in *Lta KO* mice and 3 doses of PD-1 blocking antibody were administered starting 7
152 days after tumor implantation (every 3 days). Strikingly, compared to responses in wildtype
153 (WT) mice (sham animal survival curves from SLNB study, **Figure 2A**, were plotted for
154 comparison), slowed tumor growth and improved survival from PD-1 inhibition were abolished
155 in these mice lacking LNs (**Figure 2E**), suggesting adaptive immune responses generated in LNs
156 contribute to ICB response. Further, these results suggest that LN-dependent compensatory
157 mechanisms occur after TDLN dissection to maintain anti-PD-1 responses in wild-type mice.

158 **LN dissection alters lymph drainage and promotes antigen access to distant lymphoid**
159 **organs**

160 To interrogate the mechanism by which animals that have undergone LN surgery generate ICB-
161 induced immune responses, we first measured the local transport of surrogate antigens to
162 alternative draining lymph nodes (DLNs) after SLNB or CLND. 2 million Dalton (MD) FITC-
163 dextran and 4.4 kilodalton (kD) TRITC-dextran were used as surrogate biomolecules with
164 different sizes. The dextran mixture was introduced to the 4th mammary fat pad in animals that
165 had undergone sham surgery or dissection of the IN LN (SLNB) or the IN/AX/BR LNs (CLND).
166 After 6 hours, ipsilateral IN, AX, BR LNs remaining in the relevant groups as well as all
167 contralateral IN LNs were collected for microscopic examination. In LNs, the majority of 2 MD
168 dextran was found to be aggregated in the subcapsular sinus (SCS) region—showing transport by
169 the lymphatic system—while 4.4kD dextran was sparsely distributed throughout the LN (**Figure**
170 **3A**). Small biomolecules can enter LNs via the lymph or blood circulation(45). However, our
171 data show that the large biomolecules rely heavily on the lymphatic system to arrive in the LN. 2
172 MD dextran abundance in AX LNs from SLNB animals is comparable to counterparts in IN or
173 AX LNs from sham animals (**Figure 3B**), indicating resection of IN LN does not disrupt the
174 drainage to the downstream AX LN. Interestingly, 2 MD dextran was also detected entering the
175 SCS of contralateral IN LNs in certain animals (**Figure 3C**). Compared to sham animals, there
176 was an increased incidence of 2 MD dextran drained to contralateral IN LNs of CLND animals
177 (**Figure 3B**). Inconsistent with a previous report(33), there was limited drainage from mammary
178 fat pad to BR LNs across conditions, suggesting BR LNs are not main DLNs (**Figure 3B**).
179 Nonetheless, because BR LNs are in axilla region, removing BR LN along with IN LN and AX
180 LN is a relevant approach to model CLND (basin dissection) which also removes non-DLNs(36,

181 39). Collectively, these data show that CLND disrupts the normal patterns of lymph drainage,
182 which results in lymph (and surrogate antigen) being transported to alternative LNs which can be
183 anatomically distant (**Figure 3D**).

184 Altogether, these findings are consistent with the clinical observation that breast cancer patients
185 who have undergone AX LN dissections are more likely to develop altered lymph drainage to
186 contralateral AX LNs(46). Similarly, radiation therapy can cause lymphatic drainage aberration
187 in breast cancer patients, which decreases flow to the ipsilateral axilla while increasing flow to
188 contralateral axilla(47).

189 To further test whether—beyond the mammary fat pad region—antigen access to distant LNs
190 can be enhanced when local lymphatic drainage is ablated, we performed sham surgery or
191 ipsilateral popliteal (PO), IN, AX and BR LN dissection on mice (ILND condition).
192 Subsequently, a mixture of 2MD and 4.4kD dextran was injected to the foot pad of those
193 animals. Due to this anatomic site, injection-induced antigen convection to distant sites was
194 minimized, and all LNs along the direct drainage path were absent. Similar to **Figure 3B**, we
195 discovered that 6 hours after injection, 2MD dextran was mainly located in ipsilateral PO, IN and
196 AX LNs when lymphatic drainage was intact, whereas ILND re-routed 2MD dextran transport to
197 contralateral IN and AX LNs (**Supp Figure 2**). The lack of 2MD dextran in contralateral PO
198 LNs suggests that, once taken up by lymphatic vessels of an adjacent lymphosome, the lymph
199 still follows the normal drainage patterns, and does not undergo retrograde flow or circulate
200 significantly through the blood in ILND mice (**Supp Figure 2**). In contrast, 4.4kD dextran, with
201 its smaller size was found in all remaining LNs (**Supp Figure 2**), suggesting transport through
202 the blood. The compensatory drainage phenomenon in the lower limb suggested by our data has
203 also been reported clinically. A recent indocyanine green fluorescence lymphography study

204 found that in patients with cancer treatment related lower limb lymphoedema, lower limb
205 interstitial fluid can be transported across the lower abdomen to the contralateral inguinal
206 region(48).

207 In addition to distant LNs, we found that 2MD dextran was also detectable in spleens from both
208 sham and ILND mice. 2MD dextran was more abundant in spleens of mice in the ILND
209 condition (**Figure 3E**). These large dextran molecules were mainly detected in the B cell
210 follicles and adjacent marginal zone macrophages, instead of residing in macrophage-rich red
211 pulp(49) (**Figure 3F**), indicating the potential for the generation of immune responses in the
212 spleen against antigen arising from distal tissue, compensating for the loss of DLNs.

213 **TDLN dissection stimulates immune responses in distant LNs**

214 Since distant LNs of CLND mice can be exposed to interstitial fluid from the primary tumor site,
215 we next examined whether tumor-specific immunity can be generated in these distant LNs.
216 B16F10 cells expressing ovalbumin (257-264: SIINFEKL) were implanted to sham surgery or
217 CLND mice and anti-PD-1 treatment started after 7 days. Subsequently, the spleen as well as any
218 ipsi- and contra-lateral LNs were collected for immunofluorescence and flow cytometry
219 analyses. CD8 T cell expansion was detected in ipsilateral LNs in sham surgery mice and
220 contralateral LNs in CLND mice (**Figure 4A**). Moreover, spleens in CLND animals contained an
221 equal percentage of CD8 T cells compared to the sham surgery counterparts (**Figure 4B**),
222 indicating that the immune reaction to the tumor was not confined within TDLNs. We also
223 measured the abundance of SIINFEKL-specific CD8 T cells (referred to throughout as OVA-T
224 cells) to assess tumor-specific immune responses (**Figure 4C**). Consistent with previous
225 investigations(28, 30), OVA-T cells were found to be predominantly enriched in sham surgery

226 ipsilateral LNs, whereas certain CLND contralateral LNs, but not cervical LNs, also harbored
227 high numbers of OVA-T cells (**Figure 4D**), indicating a directional spread of antigen consistent
228 with adjacent lymphosomes, instead of systemic spread . Additionally, the abundance of OVA-T
229 cells was comparable in spleens and blood of both sham and CLND mice (**Figure 4D**),
230 demonstrating that the generation of circulating tumor-specific T cells persists after LN surgery.

231 To better recapitulate the clinical situation, ICB-induced tumor-specific T cell response was
232 tested in an adjuvant setting. Two weeks after tumor implantation in intact mice, primary tumor
233 removal was performed with or without CLND. After 3 days of recovery, mice were given anti-
234 PD-1 treatment. No difference was found in OVA-T cell abundance between sham ipsilateral
235 LNs and CLND contralateral LNs (**Figure 4E**), indicating, that even without the primary tumor
236 antigen source, distant LNs can generate tumor-specific immune response after the removal of
237 the initial TDLNs. To test whether tumor-specific T cells from distant LNs can infiltrate
238 recurrent tumors, B16F10-OVA tumors were implanted into Kaede mice(50), and the tumors
239 were resected with and without CLND; the mice were then treated with adjuvant anti-PD1
240 inhibition. After 14 days, these mice were implanted with B16F10-OVA tumors in the same
241 primary site—to model recurrence—followed by photoconversion of contralateral IN LNs.
242 Strikingly, Kaede red+ OVA-T cells were present in recurrent tumors, and the abundance was
243 greater in CLND mice, compared to mice that did not undergo LN surgery (**Figure 4F**),
244 suggesting that immune cells from distant LNs can be activated and traffic to recurrent tumors.

245 Antigen can disseminate by advection with interstitial fluid, but it can also be carried by antigen-
246 presenting cells (APCs), which may access distant LNs after primary DLN resection. To assess
247 the contribution of APCs, sham surgery or dissection of PO, IN, AX and BR LNs (ILND
248 condition) was conducted in cohorts of mice. After recovery from surgery, bone marrow-derived

249 DCs (BMDCs) from donor mice were loaded with OVA, stimulated with lipopolysaccharide
250 (LPS) and subsequently injected in the foot pad of sham or ILND mice. Intriguingly, we found
251 that OVA-T cells were significantly enriched in ipsilateral LNs of sham mice and contralateral
252 LNs of ILND mice, but not contralateral LNs of sham animals (**Figure 4G**). These results
253 suggest that antigen carrying-APCs also have greater access to distant LNs when lymphatic
254 drainage is disrupted.

255 In addition to tumor-specific responses in distant LNs, the status of tumor-infiltrating T cells in
256 B16F10 tumors after CLND was measured. Compared to sham condition, ICB-induced
257 proliferating, non-exhausted CD8 effector T cells (CD44+, PD1+, Tbet+, KLRG1-, Ki67+) in
258 tumor persist after CLND (**Figure 4H, Supp Figure 3A**). Moreover, in sham and CLND mice
259 treated by ICB, we measured memory T cell populations in remaining LNs after primary tumor
260 (B16F10) resection and subsequent tumor rechallenge. Strikingly, non-exhausted stem-like
261 central memory CD8 T cells (CD44+, PD1+, CD62L+, TCF1+, CD127+, KLRG1-, Tim3-,
262 Lag3-) were similarly abundant in ipsilateral LNs of sham mice and contralateral LNs of CLND
263 mice (**Figure 4I, Supp Figure 3B**). Taken together, ICB-mediated acute tumor-infiltrating T cell
264 response and memory T cell response in remaining LNs persist after LN resection.

265 As our data show that large dextran molecules are enriched in the spleen after CLND (**Figure 3**
266 **E&F**) and accompanied by CD8 T cell expansion (**Figure 4B**) and a tumor-specific T cell
267 response (**Figure 4D**), we next determined whether the spleen is essential for residual ICB
268 response in mice after CLND. To that end, sham surgery (SP+ condition) or splenectomy (SP-
269 condition) was performed 2 weeks prior to CLND, and E0771 tumors were implanted and treated
270 as described before. Unexpectedly, splenectomy did not significantly affect the overall survival
271 in anti-PD-1 treated mice. Complete responders were less frequent, but still present, in SP- mice

272 (**Supp Figure 4A)**. Further, all complete responders (5/5) from the SP+ condition and 2 out of 3
273 of SP- counterparts could completely reject tumor rechallenge, (**Supp Figure 4B)**. Altogether,
274 these data suggest that the spleen contributes, but only marginally, to the ICB response and long-
275 term immune memory formation in CLND mice.

276 **Mathematical modeling of antigen access to adjacent lymphosomes via dermal interstitial**
277 **transport after TDLN dissection**

278 Because our data show that antigen can access adjacent lymphosomes and activate distant LNs
279 (**Figure 3&4)**, we next used mathematical modeling to help understand this process from a
280 pharmacokinetic perspective. To that end, we developed a multi-scale computational model of
281 transport of free antigen and imaging tracers **(Figure 5A&B)** that recapitulates our primary
282 experimental findings in mice and predicts how these results may translate to clinical practice in
283 humans (details of the model provided in **Supplemental Materials**).

284 Normally, a local equilibrium exists in which interstitial fluid pressure remains low—near or just
285 below atmospheric pressure—and little lateral movement of fluid occurs in the superficial tissue
286 layers. In contrast, **Figure 5C-F** shows how disabling various combinations of the IN, AX, BR,
287 and PO nodes in the mouse diverts flow to adjacent lymphosomes due to the lack of local
288 pressure minima provided by lymphatic drainage. In general, disabled collecting lymphatic
289 vessels lead to the accumulation of interstitial fluid and then its redirection to the next adjacent
290 lymphosome – even across the midline. This transport can occur through the tissue interstitial
291 space or through the non-valved, highly interconnected lymphatic capillary network. However,
292 the DLN(s) for the adjacent lymphosome might be relatively distal, helping to explain our in

293 vivo data in models of CLND. This computational model predicts that antigen can activate
294 immune responses in specific distal LNs in the body after LN resections.

295 Our results in a human model (**Figure 5G-I**) were qualitatively similar to those in mice, but
296 important differences arise because of the relative size of the lymphosomes, anatomical
297 connectivity of the vessels, and the degree of redundancy in the lymphatic networks. The
298 pressures in the skin obtained from the full, 3-D human model were compared to an analytical
299 result for a planar, circular lymphosome with the same surface area (**Figure 5J**) in **Figure 5K**.

300 To examine the size dependence of the lymphosome, we performed a parametric study of the
301 simplified model **(Figure 5L)**. Here, we found that larger lymphosomes, such as those present in
302 humans, generate more total fluid that must be drained and result in higher interstitial pressures
303 than expected in mice. This size difference alone may account for much of the relative difficulty
304 in creating experimental models of lymphedema in laboratory mice. An additional result of the
305 simplified model **(Figure 5M)** was that the mobility of the fluid (κ) in the network of initial
306 lymphatic vessels strongly affects the interstitial fluid pressure, but has little influence on the
307 total quantity of antigen-carrying fluid diverted elsewhere or its destination.

308 **Administration of ICB to distant LNs enhances efficacy after TDLN dissection**

309 Previous investigations demonstrated that directly delivering a low dose of ICB agents to TDLNs
310 can achieve robust anti-tumor responses(30, 31, 35). These findings highlight the potential of
311 LNs to be used as an ICB target site. Because distant LNs are more likely to be exposed to tumor
312 antigen after LN dissection (**Figure 3 & Supp Figure 2**), we assessed the importance of
313 contralateral LNs for low-dose ICB treatment in mice that have undergone CLND. Since anti-
314 CTLA4 and anti-PD-1 combination has shown efficacy in clinical settings(51), we delivered this

315 ICB combination at low dose (5mg/kg) by intradermal administration in a lymphatic basin that is
316 drained by ipsilateral LNs (tumor draining IN+AX) in sham LN surgery mice or contralateral
317 LNs in CLND mice. Compared to isotype IgG, we found ICB drastically increases the volume of
318 ipsilateral LNs in sham LN surgery mice and contralateral LNs in CLND mice (**Figure 6A**).
319 Additionally, these LNs share similar T cell composition (**Figure 6B**) and possess comparable
320 abundance of stem-like effector memory T cells (CD44+, PD-1+, TCF1+, CD39-, CD62L-)
321 which are key contributors to ICB response(52) (**Figure 6C**). Altogether, similar to TDLNs,
322 distant LNs can be activated by ICB in mice after CLND.

323 To directly test the potency of distant LNs during ICB treatment, we treated sham LN surgery
324 and CLND mice bearing E0771 tumors with anti-CTLA4 and anti-PD-1 antibodies (5mg/kg) by
325 intraperitoneal (IP) administration or intradermal administration to contralateral LNs (C.LNs).
326 Strikingly, compared to systemic delivery, combination ICB given to C.LNs provides greater
327 survival benefit and response rate in CLND mice, but not in sham LN surgery counterparts
328 (**Figure 6D**). These results provocatively suggest that delivering ICB therapeutics to downstream
329 or distant LNs may benefit patients that have undergone LN surgery.

330 Compared to adjuvant-only regimens, neoadjuvant-adjuvant ICB can provide better outcomes for
331 patients with advanced melanoma(53). To examine whether LN surgery compromises
332 neoadjuvant-adjuvant ICB efficacy, B16F10 tumors expressing Gaussia luciferase (B16F10-
333 Gluc) were treated with ICB delivered to the TDLN, and curative primary tumor resection with
334 or without LN surgery (SLNB or CLND) was performed (**Figure 6E**). Mice were monitored for
335 tumor recurrence and metastases (Gluc activity) for 100 days. After 100 days tumor-free mice
336 were rechallenged with B16F10-Gluc cells, and mice that developed tumors were treated with
337 adjuvant ICB delivered to the TDLN (IN LN in no LN surgery condition, AX LN in SLNB

338 condition and contralateral IN LN in CLND condition) (**Figure 6E**). Interestingly, after surgery,
339 ICB, but not IgG, induced vitiligo, especially, at the surgery sites of both primary tumor
340 resection and LN surgery (**Figure 6F**). The appearance of vitiligo indicates that the ICB-induced
341 immune response to antigens involved in melanin production disseminates beyond the primary
342 tumor location(54). After neoadjuvant treatment, only one mouse in the No LN surgery + ICB
343 condition had a spontaneous recurrent tumor and one mouse in the SLNB + ICB condition died
344 due to a cause unrelated to cancer (**Figure 6G**), demonstrating the potency of curative surgery.
345 Upon rechallenge, compared to naïve mice, all surgically treated mice exhibited immune
346 memory against the original tumors, while ICB-treated mice possessed greater immune memory
347 compared to IgG-treated counterparts (**Figure 6H**). At this sample size (~15 mice), the ICB-
348 induced immune memory and survival benefit persists after SLNB or CLND (**Figure 6H&I**).
349 Surprisingly, these results suggest that, in a TDLN targeted neoadjuvant-adjuvant ICB treatment
350 regimen, the formation of immune memory against cancer cells and improvement of overall
351 survival persist after LN surgery along with curative primary tumor resection.

352 **LN-egressing immune cells are expendable for long-term anti-tumor immune memory**

353 Complete responders emerged after ICB treatment in sham LN surgery and TDLN resected mice
354 (**Figure 2&6**). To evaluate the long-term immune memory, we re-introduced E0771 cells to the
355 original tumor sites of anti-PD1 treatment complete responders (**Figure 2**). Survivors in both
356 sham LN surgery and TDLNs removed conditions rejected tumor rechallenge (**Supp Figure 5A**).
357 To further test whether this immune memory is systemic, E0771 cells were introduced to both
358 ipsi- and contra-lateral sides of animals. Similarly, all survivors, regardless of the presence of
359 TDLNs, remained tumor-free (**Supp Figure 5B**). Finally, we determined that this immune

360 memory is tumor specific, as E0771-immune mice cannot reject B16F10 tumors implanted in
361 either mammary fat pad or dermis (**Supp Figure 5C**).

362 Lymphocytes use sphingosine 1-phosphate (S1P) signaling to exit lymphoid organs including
363 bone marrow, LNs and Peyer's patches(55-57). Indeed, FTY720, a potent inhibitor against
364 S1PR(58), treatment drastically reduced CD4, CD8 and central memory (CD44+/CD62L+) T
365 cells in the circulation ~90% (**Supp Figure 5D)**, suggesting this treatment can block T cells
366 egress from lymphoid organs including LNs. We aimed to test whether central memory T cells
367 from LNs enter the circulation and greatly contribute to long-term immune memory in tumor-
368 free survivors. To that end, tumor naïve control mice or tumor-free survivors-implanted with
369 E0771 or B16F10-Gluc tumors-generated by ICB combo treatment studies (**Figure 6**) were fed
370 with water with or without FTY720 (2.5μg/ml). Subsequently, E0771 or B16F10-Gluc tumors
371 were orthotopically implanted to both the primary tumor location and the contralateral site for re-
372 challenge. Intriguingly, the vast majority of complete ICB responders remained tumor-free,
373 while there were fewer tumor-immune mice in survivors that were cured by surgery (No LN
374 Surgery IgG condition) (**Supp Figure 5E**). Like previous observations (**Supp Figure 5A&B**),
375 LN surgery status did not affect the immune memory (**Supp Figure 5E)**. Strikingly, this anti-
376 tumor immune memory did not only reside within primary tumor tissues, as subsequent tumors
377 implanted in the ectopic sites (dermis for E0771 and mammary fat pad for B16F10-Gluc) of
378 these tumor-free survivors from the orthotopic rechallenge study were also rejected (**Supp**
379 **Figure 5F)**. These findings suggest that ICB-induced anti-tumor immune memory cells spread
380 systemically in complete responders, and the contribution of immune cells egressing from
381 lymphoid organs is dispensable after memory responses have formed.

382 **Distant LNs are reactive after resection of tumor and disease-related LNs in head and neck**
383 **cancer patients treated by ICB**

384 To test whether, after LN dissection, distant LNs contribute to ICB efficacy on suppressing
385 cancer recurrence in patients, we investigated head and neck cancer patients treated by ICB that
386 tend to have a high local recurrence rate(59). We examined a recent phase I/Ib trial
387 (NCT03635164) in which HPV negative head and neck cancer patients that received neoadjuvant
388 treatment to manage gross disease (primary and grossly involved nodes) consisting of
389 combination hypofractionated radiotherapy and durvalumab (targeting PD-L1). Following a
390 recovery time ranging from 5-6 weeks in the extension cohort, patients underwent surgical
391 resection of the primary tumor and bilateral neck dissection per standard of care. Those with
392 major pathological response or complete pathological response to neoadjuvant radiotherapy and
393 durvalumab were classified as responders (response>95%). Under permission of multi-
394 disciplinary tumor board, with the exception of four cycles of durvalumab, all other adjuvant
395 therapy in the form of radiation or chemotherapy was omitted in responders(60). To date, no
396 recurrent disease was detected in these responders during post-operative follow-up visits (>2
397 years). We compared CT and PET images at diagnosis to post-surgery follow-up examinations in
398 the responder cohort. Strikingly, after removal of the tumor and initial TDLNs, enlargement of
399 distant LNs was found in most responders, but not in non-responders (**Figure 7A**). Of note, no
400 nodal disease was detected by radiology-guided biopsy, indicating these enlarged LNs were
401 activated and immune-reactive. The reactive LNs were higher echelon LNs in areas that were
402 now draining the original tumor site. For instance, in patients 01-013 and 01-015, lower neck
403 LNs (posterior cervical) and upper neck LNs (submandibular and submental) were enlarged,
404 respectively, at follow-up, which was not observed at diagnosis (**Figure 7B**). Similarly, in

405 patient 01-009, neck draining mediastinal LNs above the aortic arch were inflamed after tumor
406 and LN resection (**Figure 7C**). These data suggest that surgical removal of the primary tumor
407 and TDLNs can result in reactive distant LNs and extend ICB response in patients.

408 **DISCUSSION:**

409 TDLNs are exposed to high antigen burden, allowing them to readily generate adaptive immune
410 response against cancer cells(17). Recent reports using mouse tumor models advocate that
411 TDLNs are indispensable for ICB response(29, 32, 33, 61), likely due to unique tumor-specific T
412 cell memory populations(29). A phase II trial (NCT03698019) of patients with resectable stage
413 III or stage IV melanoma, neoadjuvant-adjuvant pembrolizumab treatment provided improved
414 event-free survival compared to adjuvant-only setting(53), indicating the presence of the primary
415 tumor and/or related LNs is important for optimal ICB response. However, clinical trials
416 involving patients with completely resected stage IIIb/c or stage IV melanoma, demonstrate that
417 patients still benefit from ICB treatment after sentinel LNs and bulky disease-related LNs
418 removal(62-64), arguing TDLNs are not necessary for ICB response. Further, retrospective
419 analysis of stage III melanoma patients demonstrates that patients benefited similarly from
420 adjuvant ICB, regardless of the extent of LN surgery. Recent work from our lab and others has
421 shown that metastatic TDLNs are immune suppressed and can impair systemic anti-cancer
422 immune responses(18-20). Ultimately, the metastatic burden in TDLNs may determine whether
423 SLNB or CLND has a positive, negative or neutral effect on disease recurrence and survival.
424 Because human LN chains are complex with multiple echelons(65), it is key to determine
425 immune activation or suppression status of LNs downstream of sentinel LNs. Identifying LNs

426 with sufficient exposure to antigen but not suppressive factors from tumor, may identify optimal
427 target sites for immunotherapy delivery.

428 In this study, we emphasize the dynamic and adaptive aspect of antigen transportation.
429 Disruption of normal lymphatic drainage drives the antigen-carrying fluid to flow to adjacent
430 lymphosomes and induces immune response in the LNs of that lymphosome. Often these LNs
431 could be quite distant (and thus non-intuitive) from the original TDLNs, which is corroborated
432 by clinical observations(46, 47). However, the maximal transport distance of interstitial antigens,
433 without being substantially diluted and degraded, remains to be determined. Further, limits of
434 active transport of APCs from the tumor site are also indeterminate. Understanding these spatial
435 limits can explain the anatomic distribution of LNs for regional immune surveillance.
436 Intriguingly, we found CLND induces tumor-specific T cells enrichment in distant LNs, when
437 performed along with primary tumor resection (adjuvant setting). The antigen source fueling the
438 tumor-specific T cell response in distant LNs is unknown. Conceivably, antigens were vastly
439 spread by the surgery, from residual cancer cells at the primary tumor site, or in occult metastatic
440 sites. Despite the importance of antigen trafficking to distant LNs, direct T cell priming in the
441 local tumor microenvironment(66) and tertiary lymphoid structures(67) may also contribute to
442 residual ICB response.

443 The finding that long-term anti-tumor immune memory is not predominantly reliant on the T cell
444 egress from LNs (**Supp Figure 5**), leads to critical unanswered questions. Do anti-tumor
445 immune memory cells disseminate from TDLNs immediately and accumulate systemically
446 during ICB? Or is systemic immune memory mainly formed after primary tumor clearance? Our
447 neoadjuvant-adjuvant ICB study (**Figure 6**) demonstrated that mice that underwent curative
448 surgery had systemic immune memory development, indicating immune reactions are present at

449 the time of tumor resection. This also suggests that adjuvant ICB may act through existing anti-
450 tumor tissue-resident immune memory cells at the time of treatment. One caveat of the FTY720
451 experiment to block T cell egress, including memory T cell egress, from LNs is that tissue-
452 resident memory cells can enter the circulation and reject tumor cells at distant sites(68). S1P
453 inhibition mainly blocks lymphocytes egress from LNs and bone marrow(55) not other tissues,
454 and circulating memory cells are still present in FTY720 treated mice. It is possible a small
455 number of cancer-specific memory clones are sufficient to suppress recurrence.

456 Additional limitations are present in our preclinical model when used to address clinical
457 questions(69). In this work, surgery of skin LNs in mice was used to recapitulate SLNB and
458 CLND procedures. However, large scale and anatomical differences are present between humans
459 and mice. On one hand, the size of a mouse is comparable to a human axilla, thus, the murine
460 version of CLND used in this work may be similar to a SLNB scenario in patients. On the other
461 hand, compared to simple chains of a few LNs in mice, humans have more complex and
462 interconnected lymphatic networks as well as multiple LNs draining one common region(65);
463 hence, removing a single LN in mice may equate to CLND in human. Encouragingly, consistent
464 with our preclinical data, compensatory lymphatic drainage(46, 47), even in the presence of
465 lymphedema(48, 70), and distant LN activation are observed in cancer patients (**Figure 7)**.
466 Further, it is important to investigate lymphatic drainage patterns after non-skin LN dissection as
467 ICB treatment increases survival in non-small cell lung cancer(71) and colorectal cancer(72)
468 patients. Finally, dissection is performed on SLNs and metastatic LNs which are
469 immunosuppressed(73) with disrupted CD8 T cell responses(74). Consequently, the net benefit
470 of removing these immune suppressive LNs is likely to outweigh the marginal decrease in
471 systemic response to ICB.

MATERIALS AND METHODS:

In Supplementary materials.

List of Supplemental Materials:

Materials and Methods.

Figure S1 to S4 for multiple supplementary figures.

References (75-85).

478 **REFERENCES:**

479 1. Ishida Y, Agata Y, Shibahara K, Honjo T. Induced expression of PD-1, a novel member
480 of the immunoglobulin gene superfamily, upon programmed cell death. EMBO J.
481 1992;11(11):3887-95.
482 2. Iwai Y, Ishida M, Tanaka Y, Okazaki T, Honjo T, Minato N. Involvement of PD-L1 on
483 tumor cells in the escape from host immune system and tumor immunotherapy by PD-L1
484 blockade. Proc Natl Acad Sci U S A. 2002;99(19):12293-7.
485 3. Brunet JF, Denizot F, Luciani MF, Roux-Dosseto M, Suzan M, Mattei MG, et al. A new
486 member of the immunoglobulin superfamily--CTLA-4. Nature. 1987;328(6127):267-70.
487 4. Leach DR, Krummel MF, Allison JP. Enhancement of antitumor immunity by CTLA-4
488 blockade. Science. 1996;271(5256):1734-6.
489 5. Hargadon KM, Johnson CE, Williams CJ. Immune checkpoint blockade therapy for
490 cancer: An overview of FDA-approved immune checkpoint inhibitors. Int Immunopharmacol.
491 2018;62:29-39.
492 6. Wei SC, Duffy CR, Allison JP. Fundamental Mechanisms of Immune Checkpoint
493 Blockade Therapy. Cancer Discov. 2018;8(9):1069-86.
494 7. Hodi FS, O'Day SJ, McDermott DF, Weber RW, Sosman JA, Haanen JB, et al. Improved
495 survival with ipilimumab in patients with metastatic melanoma. N Engl J Med. 2010;363(8):711-
496 23.
497 8. Robert C, Long GV, Brady B, Dutriaux C, Maio M, Mortier L, et al. Nivolumab in
498 previously untreated melanoma without BRAF mutation. N Engl J Med. 2015;372(4):320-30.
499 9. Borghaei H, Paz-Ares L, Horn L, Spigel DR, Steins M, Ready NE, et al. Nivolumab
500 versus Docetaxel in Advanced Nonsquamous Non-Small-Cell Lung Cancer. N Engl J Med.
501 2015;373(17):1627-39.
502 10. Brahmer J, Reckamp KL, Baas P, Crino L, Eberhardt WE, Poddubskaya E, et al.
503 Nivolumab versus Docetaxel in Advanced Squamous-Cell Non-Small-Cell Lung Cancer. N Engl
504 J Med. 2015;373(2):123-35.
505 11. Motzer RJ, Tannir NM, McDermott DF, Aren Frontera O, Melichar B, Choueiri TK, et
506 al. Nivolumab plus Ipilimumab versus Sunitinib in Advanced Renal-Cell Carcinoma. N Engl J
507 Med. 2018;378(14):1277-90.
508 12. Chen R, Zinzani PL, Fanale MA, Armand P, Johnson NA, Brice P, et al. Phase II Study
509 of the Efficacy and Safety of Pembrolizumab for Relapsed/Refractory Classic Hodgkin
510 Lymphoma. J Clin Oncol. 2017;35(19):2125-32.
511 13. El-Khoueiry AB, Sangro B, Yau T, Crocenzi TS, Kudo M, Hsu C, et al. Nivolumab in
512 patients with advanced hepatocellular carcinoma (CheckMate 040): an open-label, non-
513 comparative, phase 1/2 dose escalation and expansion trial. Lancet. 2017;389(10088):2492-502.
514 14. Duffy AG, Ulahannan SV, Makorova-Rusher O, Rahma O, Wedemeyer H, Pratt D, et al.
515 Tremelimumab in combination with ablation in patients with advanced hepatocellular carcinoma.
516 J Hepatol. 2017;66(3):545-51.
517 15. Janjigian YY, Shitara K, Moehler M, Garrido M, Salman P, Shen L, et al. First-line
518 nivolumab plus chemotherapy versus chemotherapy alone for advanced gastric, gastro-
519 oesophageal junction, and oesophageal adenocarcinoma (CheckMate 649): a randomised, open-
520 label, phase 3 trial. Lancet. 2021;398(10294):27-40.
521 16. Padera TP, Meijer EF, Munn LL. The Lymphatic System in Disease Processes and
522 Cancer Progression. Annu Rev Biomed Eng. 2016;18:125-58.

17. Zhou H, Lei PJ, Padera TP. Progression of Metastasis through Lymphatic System. Cells. 2021;10(3).
18. Jones D, Wang Z, Chen IX, Zhang S, Banerji R, Lei PJ, et al. Solid stress impairs lymphocyte infiltration into lymph-node metastases. Nat Biomed Eng. 2021;5(12):1426-36.
19. Lei PJ, Pereira ER, Andersson P, Amoozgar Z, Van Wijnbergen JW, O'Melia MJ, et al. Cancer cell plasticity and MHC-II-mediated immune tolerance promote breast cancer metastasis to lymph nodes. J Exp Med. 2023;220(9).
20. Reticker-Flynn NE, Zhang W, Belk JA, Basto PA, Escalante NK, Pilarowski GOW, et al. Lymph node colonization induces tumor-immune tolerance to promote distant metastasis. Cell. 2022;185(11):1924-42 e23.
21. Brown M, Assen FP, Leithner A, Abe J, Schachner H, Asfour G, et al. Lymph node blood vessels provide exit routes for metastatic tumor cell dissemination in mice. Science. 2018;359(6382):1408-11.
22. Pereira ER, Kedrin D, Seano G, Gautier O, Meijer EFJ, Jones D, et al. Lymph node metastases can invade local blood vessels, exit the node, and colonize distant organs in mice. Science. 2018;359(6382):1403-7.
23. Alatengbaolide, Lin D, Li Y, Xu H, Chen J, Wang B, et al. Lymph node ratio is an independent prognostic factor in gastric cancer after curative resection (R0) regardless of the examined number of lymph nodes. Am J Clin Oncol. 2013;36(4):325-30.
24. Aoyama T, Yamamoto N, Kamiya M, Murakawa M, Tamagawa H, Sawazaki S, et al. The Lymph Node Ratio Is an Independent Prognostic Factor in Pancreatic Cancer Patients Who Receive Curative Resection Followed by Adjuvant Chemotherapy. Anticancer Res. 2018;38(8):4877-82.
25. Chen CC, Lin JC, Chen KW. Lymph node ratio as a prognostic factor in head and neck cancer patients. Radiat Oncol. 2015;10:181.
26. Scoggins CR, Bowen AL, Martin RC, 2nd, Edwards MJ, Reintgen DS, Ross MI, et al. Prognostic information from sentinel lymph node biopsy in patients with thick melanoma. Arch Surg. 2010;145(7):622-7.
27. Voordeckers M, Vinh-Hung V, Van de Steene J, Lamote J, Storme G. The lymph node ratio as prognostic factor in node-positive breast cancer. Radiother Oncol. 2004;70(3):225-30.
28. Dammeijer F, van Gulijk M, Mulder EE, Lukkes M, Klaase L, van den Bosch T, et al. The PD-1/PD-L1-Checkpoint Restrains T cell Immunity in Tumor-Draining Lymph Nodes. Cancer Cell. 2020;38(5):685-700 e8.
29. Huang Q, Wu X, Wang Z, Chen X, Wang L, Lu Y, et al. The primordial differentiation of tumor-specific memory CD8(+) T cells as bona fide responders to PD-1/PD-L1 blockade in draining lymph nodes. Cell. 2022.
30. Francis DM, Manspeaker MP, Schudel A, Sestito LF, O'Melia MJ, Kissick HT, et al. Blockade of immune checkpoints in lymph nodes through locoregional delivery augments cancer immunotherapy. Sci Transl Med. 2020;12(563).
31. O'Melia MJ, Manspeaker MP, Thomas SN. Tumor-draining lymph nodes are survival niches that support T cell priming against lymphatic transported tumor antigen and effects of immune checkpoint blockade in TNBC. Cancer Immunol Immunother. 2021;70(8):2179-95.
32. Fransen MF, Schoonderwoerd M, Knopf P, Camps MG, Hawinkels LJ, Kneilling M, et al. Tumor-draining lymph nodes are pivotal in PD-1/PD-L1 checkpoint therapy. JCI Insight. 2018;3(23).

33. Zhao X, Kassaye B, Wangmo D, Lou E, Subramanian S. Chemotherapy but Not the Tumor Draining Lymph Nodes Determine the Immunotherapy Response in Secondary Tumors. iScience. 2020;23(5):101056.
34. Eggermont AM, Chiarion-Sileni V, Grob JJ, Dummer R, Wolchok JD, Schmidt H, et al. Adjuvant ipilimumab versus placebo after complete resection of high-risk stage III melanoma (EORTC 18071): a randomised, double-blind, phase 3 trial. Lancet Oncol. 2015;16(5):522-30.
35. van Pul KM, Notohardjo JCL, Fransen MF, Koster BD, Stam AGM, Chondronasiou D, et al. Local delivery of low-dose anti-CTLA-4 to the melanoma lymphatic basin leads to systemic Treg reduction and effector T cell activation. Sci Immunol. 2022;7(73):eabn8097.
36. Faries MB, Thompson JF, Cochran AJ, Andtbacka RH, Mozzillo N, Zager JS, et al. Completion Dissection or Observation for Sentinel-Node Metastasis in Melanoma. N Engl J Med. 2017;376(23):2211-22.
37. Cheng A, Lang J. Survival Analysis of Lymph Node Resection in Ovarian Cancer: A Population-Based Study. Front Oncol. 2020;10:355.
38. Gortzak-Uzan L, Jimenez W, Nofech-Mozes S, Ismiil N, Khalifa MA, Dube V, et al. Sentinel lymph node biopsy vs. pelvic lymphadenectomy in early stage cervical cancer: is it time to change the gold standard? Gynecol Oncol. 2010;116(1):28-32.
39. Veronesi U, Paganelli G, Viale G, Luini A, Zurrida S, Galimberti V, et al. A randomized comparison of sentinel-node biopsy with routine axillary dissection in breast cancer. N Engl J Med. 2003;349(6):546-53.
40. Nakajima Y, Asano K, Mukai K, Urai T, Okuwa M, Sugama J, et al. Near-Infrared Fluorescence Imaging Directly Visualizes Lymphatic Drainage Pathways and Connections between Superficial and Deep Lymphatic Systems in the Mouse Hindlimb. Sci Rep. 2018;8(1):7078.
41. De Togni P, Goellner J, Ruddle NH, Streeter PR, Fick A, Mariathasan S, et al. Abnormal development of peripheral lymphoid organs in mice deficient in lymphotoxin. Science. 1994;264(5159):703-7.
42. Banks TA, Rouse BT, Kerley MK, Blair PJ, Godfrey VL, Kuklin NA, et al. Lymphotoxin-alpha-deficient mice. Effects on secondary lymphoid organ development and humoral immune responsiveness. J Immunol. 1995;155(4):1685-93.
43. Mariathasan S, Matsumoto M, Baranyay F, Nahm MH, Kanagawa O, Chaplin DD. Absence of lymph nodes in lymphotoxin-alpha(LT alpha)-deficient mice is due to abnormal organ development, not defective lymphocyte migration. J Inflamm. 1995;45(1):72-8.
44. Davis IA, Rouse BT. Immune responsiveness of lymphotoxin-alpha-deficient mice: two reconstitution models. Cell Immunol. 1998;189(2):116-24.
45. Meijer EFJ, Blatter C, Chen IX, Bouta E, Jones D, Pereira ER, et al. Lymph node effective vascular permeability and chemotherapy uptake. Microcirculation. 2017;24(6).
46. Maaskant-Braat AJ, de Bruijn SZ, Woensdregt K, Pijpers H, Voogd AC, Nieuwenhuijzen GA. Lymphatic mapping after previous breast surgery. Breast. 2012;21(4):444-8.
47. Sato A, Sakai T, Iwase T, Kano F, Kimura K, Ogiya A, et al. Altered lymphatic drainage patterns in re-operative sentinel lymph node biopsy for ipsilateral breast tumor recurrence. Radiat Oncol. 2019;14(1):159.
48. Suami H, Thompson B, Mackie H, Blackwell R, Heydon-White A, Blake FT, et al. A new indocyanine green fluorescence lymphography protocol for diagnostic assessment of lower limb lymphoedema. J Plast Reconstr Aesthet Surg. 2022.

613 49. Bronte V, Pittet MJ. The spleen in local and systemic regulation of immunity. Immunity.
614 2013;39(5):806-18.
615 50. Tomura M, Yoshida N, Tanaka J, Karasawa S, Miwa Y, Miyawaki A, et al. Monitoring
616 cellular movement in vivo with photoconvertible fluorescence protein "Kaede" transgenic mice.
617 Proc Natl Acad Sci U S A. 2008;105(31):10871-6.
618 51. Wolchok JD, Chiarion-Sileni V, Gonzalez R, Grob JJ, Rutkowski P, Lao CD, et al. Long-
619 Term Outcomes With Nivolumab Plus Ipilimumab or Nivolumab Alone Versus Ipilimumab in
620 Patients With Advanced Melanoma. J Clin Oncol. 2022;40(2):127-37.
621 52. Siddiqui I, Schaeuble K, Chennupati V, Fuertes Marraco SA, Calderon-Copete S, Pais
622 Ferreira D, et al. Intratumoral Tcf1(+)PD-1(+)CD8(+) T Cells with Stem-like Properties Promote
623 Tumor Control in Response to Vaccination and Checkpoint Blockade Immunotherapy.
624 Immunity. 2019;50(1):195-211 e10.
625 53. Patel SP, Othus M, Chen Y, Wright GP, Jr., Yost KJ, Hyngstrom JR, et al. Neoadjuvant-
626 Adjuvant or Adjuvant-Only Pembrolizumab in Advanced Melanoma. N Engl J Med.
627 2023;388(9):813-23.
628 54. Lo JA, Kawakubo M, Juneja VR, Su MY, Erlich TH, LaFleur MW, et al. Epitope
629 spreading toward wild-type melanocyte-lineage antigens rescues suboptimal immune checkpoint
630 blockade responses. Sci Transl Med. 2021;13(581).
631 55. Baeyens A, Fang V, Chen C, Schwab SR. Exit Strategies: S1P Signaling and T Cell
632 Migration. Trends Immunol. 2015;36(12):778-87.
633 56. Cyster JG, Schwab SR. Sphingosine-1-phosphate and lymphocyte egress from lymphoid
634 organs. Annu Rev Immunol. 2012;30:69-94.
635 57. Girard JP, Moussion C, Forster R. HEVs, lymphatics and homeostatic immune cell
636 trafficking in lymph nodes. Nat Rev Immunol. 2012;12(11):762-73.
637 58. Brinkmann V, Cyster JG, Hla T. FTY720: sphingosine 1-phosphate receptor-1 in the
638 control of lymphocyte egress and endothelial barrier function. Am J Transplant. 2004;4(7):1019-
639 25.
640 59. Borsetto D, Sethi M, Polesel J, Tomasoni M, Deganello A, Nicolai P, et al. The risk of
641 recurrence in surgically treated head and neck squamous cell carcinomas: a conditional
642 probability approach. Acta Oncol. 2021;60(7):942-7.
643 60. Darragh LB, Knitz MM, Hu J, Clambey ET, Backus J, Dumit A, et al. A phase I/Ib trial
644 and biological correlate analysis of neoadjuvant SBRT with single-dose durvalumab in HPV-
645 unrelated locally advanced HNSCC. Nat Cancer. 2022;3(11):1300-17.
646 61. Saddawi-Konefka R, O'Farrell A, Faraji F, Clubb L, Allevato MM, Jensen SM, et al.
647 Lymphatic-preserving treatment sequencing with immune checkpoint inhibition unleashes
648 cDC1-dependent antitumor immunity in HNSCC. Nat Commun. 2022;13(1):4298.
649 62. Weber J, Mandala M, Del Vecchio M, Gogas HJ, Arance AM, Cowey CL, et al.
650 Adjuvant Nivolumab versus Ipilimumab in Resected Stage III or IV Melanoma. N Engl J Med.
651 2017;377(19):1824-35.
652 63. Ascierto PA, Del Vecchio M, Mandala M, Gogas H, Arance AM, Dalle S, et al. Adjuvant
653 nivolumab versus ipilimumab in resected stage IIIB-C and stage IV melanoma (CheckMate 238):
654 4-year results from a multicentre, double-blind, randomised, controlled, phase 3 trial. Lancet
655 Oncol. 2020;21(11):1465-77.
656 64. Weber JS, Schadendorf D, Del Vecchio M, Larkin J, Atkinson V, Schenker M, et al.
657 Adjuvant Therapy of Nivolumab Combined With Ipilimumab Versus Nivolumab Alone in

Patients With Resected Stage IIIB-D or Stage IV Melanoma (CheckMate 915). J Clin Oncol. 2022:JCO2200533.
65. Haley PJ. The lymphoid system: a review of species differences. J Toxicol Pathol. 2017;30(2):111-23.
66. Fu C, Jiang A. Dendritic Cells and CD8 T Cell Immunity in Tumor Microenvironment. Front Immunol. 2018;9:3059.
67. Bery AI, Shepherd HM, Li W, Krupnick AS, Gelman AE, Kreisel D. Role of tertiary lymphoid organs in the regulation of immune responses in the periphery. Cellular and molecular life sciences : CMLS. 2022;79(7):359.
68. Wijeyesinghe S, Beura LK, Pierson MJ, Stolley JM, Adam OA, Ruscher R, et al. Expansible residence decentralizes immune homeostasis. Nature. 2021;592(7854):457-62.
69. Perlman RL. Mouse models of human disease: An evolutionary perspective. Evol Med Public Health. 2016;2016(1):170-6.
70. Heydon-White A, Suami H, Boyages J, Koelmeyer L, Peebles KC. Assessing breast lymphoedema following breast cancer treatment using indocyanine green lymphography. Breast Cancer Res Treat. 2020;181(3):635-44.
71. Onoi K, Chihara Y, Uchino J, Shimamoto T, Morimoto Y, Iwasaku M, et al. Immune Checkpoint Inhibitors for Lung Cancer Treatment: A Review. J Clin Med. 2020;9(5).
72. Boukouris AE, Theochari M, Stefanou D, Papalambros A, Felekouras E, Gogas H, et al. Latest evidence on immune checkpoint inhibitors in metastatic colorectal cancer: A 2022 update. Crit Rev Oncol Hematol. 2022;173:103663.
73. Jones D, Pereira ER, Padera TP. Growth and Immune Evasion of Lymph Node Metastasis. Front Oncol. 2018;8:36.
74. Rahim MK, Okholm TLH, Jones KB, McCarthy EE, Liu CC, Yee JL, et al. Dynamic CD8(+) T cell responses to cancer immunotherapy in human regional lymph nodes are disrupted in metastatic lymph nodes. Cell. 2023;186(6):1127-43 e18.
75. CoreTeam R. R: A language and environment for statistical computing. R Foundation for Statistical Computing, Vienna, Austria 2021.
76. Wurdinger T, Badr C, Pike L, de Kleine R, Weissleder R, Breakefield XO, et al. A secreted luciferase for ex vivo monitoring of in vivo processes. Nat Methods. 2008;5(2):171-3.
77. Savinkov R, Grebennikov D, Puchkova D, Chereshnev V, Sazonov I, Bocharov G. Graph Theory for Modeling and Analysis of the Human Lymphatic System. Mathematics. 2020;8(12):2236.
78. Grebennikov D, Savinkov R, Zelenova E, Lobov G, Bocharov G. Network Modeling of Murine Lymphatic System. Algorithms. 2023;16(3):168.
79. Kawashima Y, Sugimura M, Hwang Y-C, Kudo N. THE LYMPH SYSTEM IN MICE. Japanese Journal of Veterinary Research. 1964;12(4):69-78.
80. Van den Broeck W, Derore A, Simoens P. Anatomy and nomenclature of murine lymph nodes: Descriptive study and nomenclatory standardization in BALB/cAnNCrl mice. J Immunol Methods. 2006;312(1-2):12-9.
81. Harrell MI, Iritani BM, Ruddell A. Lymph node mapping in the mouse. J Immunol Methods. 2008;332(1-2):170-4.
82. Suami H, Scaglioni MF. Lymphatic Territories (Lymphosomes) in the Rat: An Anatomical Study for Future Lymphatic Research. Plast Reconstr Surg. 2017;140(5):945-51.
83. Truskey GA, Yuan F, Katz DF. Transport phenomena in biological systems. 2nd edition ed: Pearson Prentice Hall; 2009.

84. Baxter LT, Jain RK. Transport of fluid and macromolecules in tumors. I. Role of interstitial pressure and convection. Microvasc Res. 1989;37(1):77-104.
85. Swartz MA, Kaipainen A, Netti PA, Brekken C, Boucher Y, Grodzinsky AJ, et al. Mechanics of interstitial-lymphatic fluid transport: theoretical foundation and experimental validation. J Biomech. 1999;32(12):1297-307.

ACKNOWLEDGEMENT

Funding:

National Institutes of Health grant K00CA234940 (H.Z.)

National Institutes of Health grant R21AI097745 (T.P.P.)

National Institutes of Health grant R01CA214913 (T.P.P.)

National Institutes of Health grant R01HL128168 (T.P.P.)

National Institutes of Health grant R01CA284372 (T.P.P.)

National Institutes of Health grant R01CA284603 (T.P.P., L.L.M. and J.W.B.)

National Institutes of Health grant R01DE028529 (S.D.K.)

National Institutes of Health grant R01DE028282 (S.D.K.)

National Institutes of Health grant R01DE028529 (S.D.K.)

National Institutes of Health grant P50CA261605 (S.D.K.)

National Institutes of Health grant R35CA242379 (M.G.V.H.)

The Rullo Family MGH Research Scholar Award (T.P.P.; G.M.B.)

The Patricia K. Donahoe Award from the Huiying Foundation (G.M.B.)

The Adelson Medical Research Foundation (G.M.B.),

The Ludwig Center at MIT (M.G.V.H.)

The MIT Center for Precision Cancer Medicine (M.G.V.H.)

The Breast Cancer Alliance (J.M.U.)

The Melanoma Research Foundation (J.M.U.).

Competing Interests:

H.Z. acknowledges that he is a scientific advisor for AOA dx. M.G.V.H. acknowledges that he is a scientific advisor for Agios Pharmaceuticals, iTeos Therapeutics, Sage Therapeutics, Pretzel Therapeutics, Lime Therapeutics, Auron Therapeutics, and Droia Ventures. G.M.B has sponsored research agreements through her institution with: Olink Proteomics, Teiko Bio, InterVenn Biosciences, Palleon Pharmaceuticals. She served on advisory boards for: Iovance, Merck, Nektar Therapeutics, Novartis, and Ankyra Therapeutics. She consults for: Merck, InterVenn Biosciences, Iovance, and Ankyra Therapeutics. She holds equity in Ankyra Therapeutics. The Phase I/Ib clinical trial NCT03635164 was funded by AstraZeneca, S.D.K also received clinical trial funding from Genentech and preclinical funding from Roche.

Author Contributions:

Conceptualization: H.Z., J.W.B., M.G.V.H., L.L.M., G.M.B., S.C., S.D.K., T.P.P.

Methodology: H.Z., J.W.B., M.G.V.H., L.L.M., G.M.B., S.C., S.D.K., T.P.P.

Data acquisition: H.Z., J.W.B., M.J.O., L.B.D., E.S., J.C., P.J.L., L.M., J.J.R.

Intellectual input: H.Z., J.W.B., M.J.O., P.J.L., L.M., M.R.N., M.S.R., M.G.V.H., J.M.U., L.L.M., G.M.B., S.C., S.D.K., T.P.P.

Project administration: H.Z., T.P.P.

Supervision: G.M.B., S.C., S.D.K., M.G.V.H., T.P.P.

Writing: H.Z., J.W.B., M.J.O., P.J.L., L.M., M.G.V.H., J.M.U., L.L.M., G.M.B., S.C., S.D.K., T.P.P.

Data and materials availability:

The data generated in this study are available within the article and its supplementary data files. The raw clinical imaging data and other clinical data, beyond what is presented in the figures in this study, are not publicly available due to the need to protect patient information.

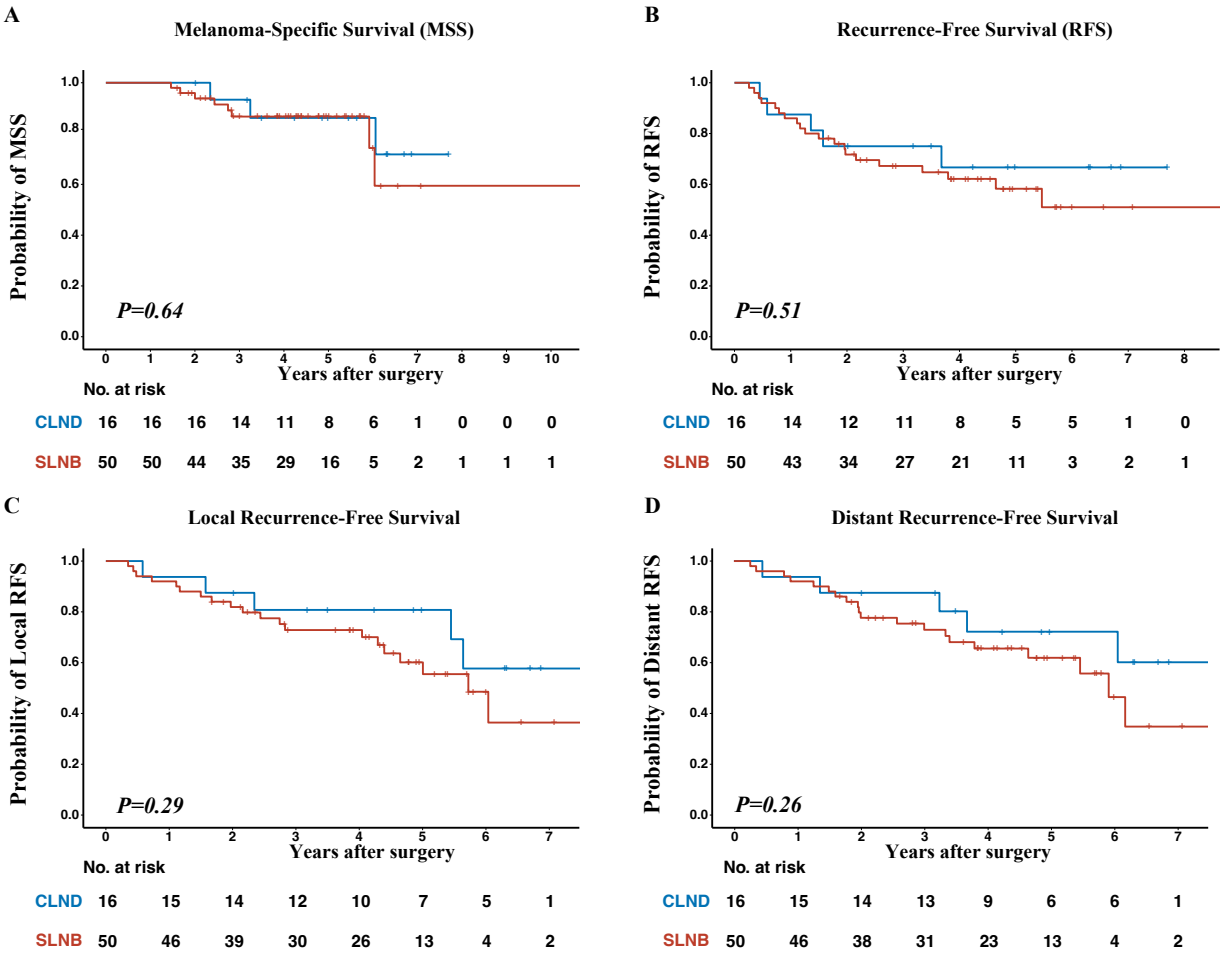

Figure 1. Adjuvant ICB response persists in stage III melanoma patients after LN surgery. Retrospective analysis was performed on a cohort of cutaneous stage III melanoma patients who underwent SLNB or CLND, and were treated by adjuvant nivolumab or pembrolizumab at Massachusetts General Hospital. (**A**) Melanoma-specific survival, (**B**) recurrence-free survival, (**C**) local recurrence-free survival and (**D**) distant recurrence-free survival are plotted.

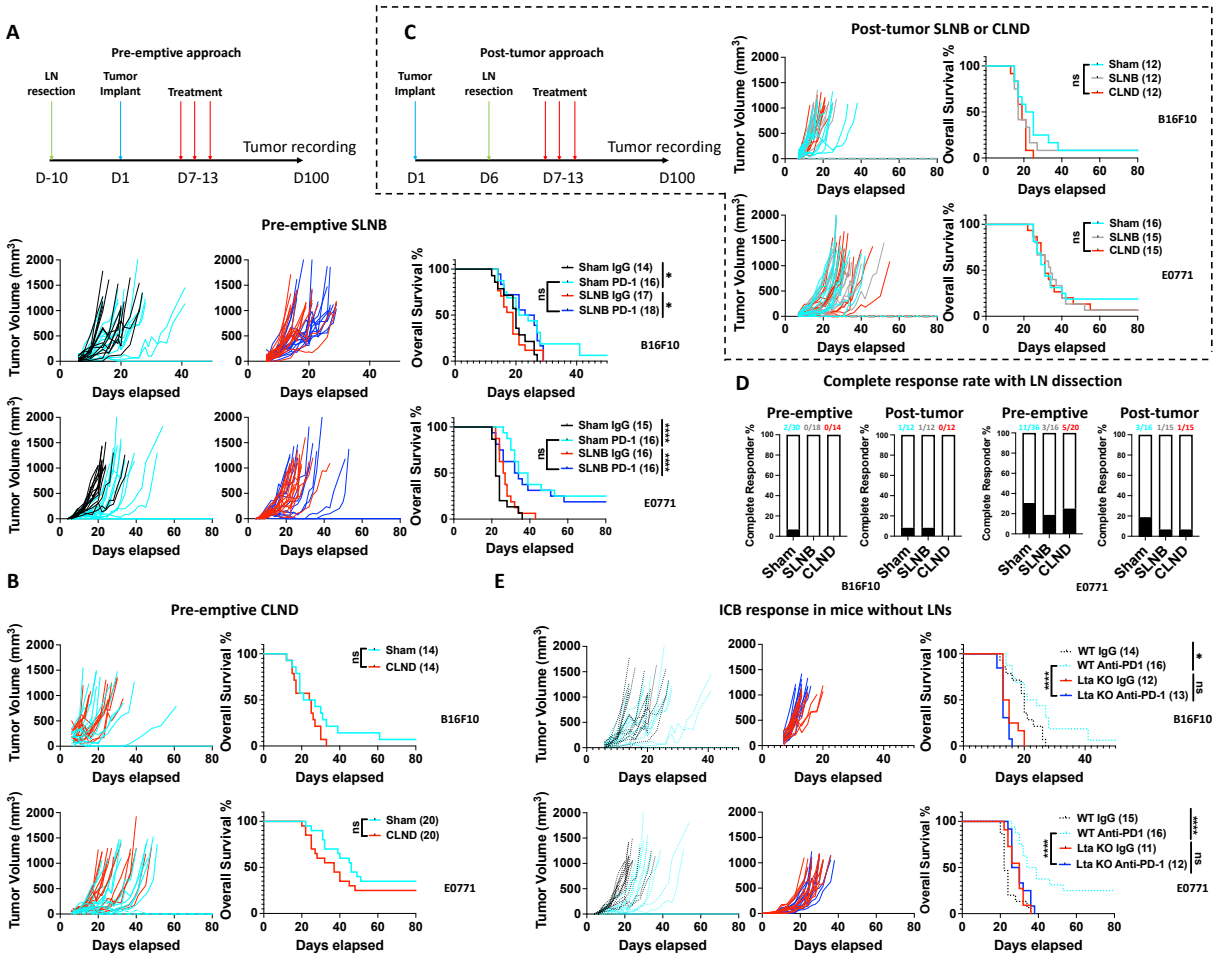

Figure 2. ICB response persists after LN dissection. (**A**) Sham surgery or SLNB was performed on C57Bl6 mice (day -10) prior to orthotopic tumor implantation (day 1). Mice were treated by rat IgG control or anti-PD1 antibody (day 7) three times (every 2 days for B16F10 or every 3 days for E0771, 10mg/kg). Tumor volume (*left & middle*) and overall survival (*right*) were plotted for mice bearing orthotopic B16F10 (*top*) or E0771 (*bottom*) tumors, respectively. (**B**) To evaluate the impact of more aggressive surgery, sham surgery or CLND was performed followed by tumor implantation and subsequent anti-PD1 inhibition using the same regimen described above. Tumor volume (*left*) and overall survival (*right*) were plotted for mice bearing B16F10 (*top*) or E0771 (*bottom*) tumors, respectively. (**C**) In contrast with pre-emptive approach, impact of post-tumor implantation LN dissection was also assessed. After tumor implantation (day 1), sham surgery, SLNB or CLND was performed on C57Bl6 mice (day 6)

774 right before anti-PD1 treatment (day 7). Tumor volume (*left*) and overall survival (*right*) were
775 plotted for mice bearing B16F10 (*top*) and E0771 (*bottom*) tumors. (**D**) Frequency of complete
776 responders from pre-emptive and post-tumor TDLN removal studies were plotted. Fisher's exact
777 test was used for statistical analysis. (**E**) B16F10 (*top*) or E0771 (*bottom*) tumor response to anti-
778 PD1 treatment was tested in Lta^{tm1Dc} mice. ICB response of wildtype (WT) sham mice from (**A**)
779 SLNB study was plotted in dashed lines for comparison. Tumor volume (*left*) and overall
780 survival (*right*) were plotted. In all animal studies, "(n)" indicates number of mice used. Log-
781 rank test with Bonferroni test was used for statistical analysis of survival data. *$p<0.05$,
782 ****$p<0.0001$.
783

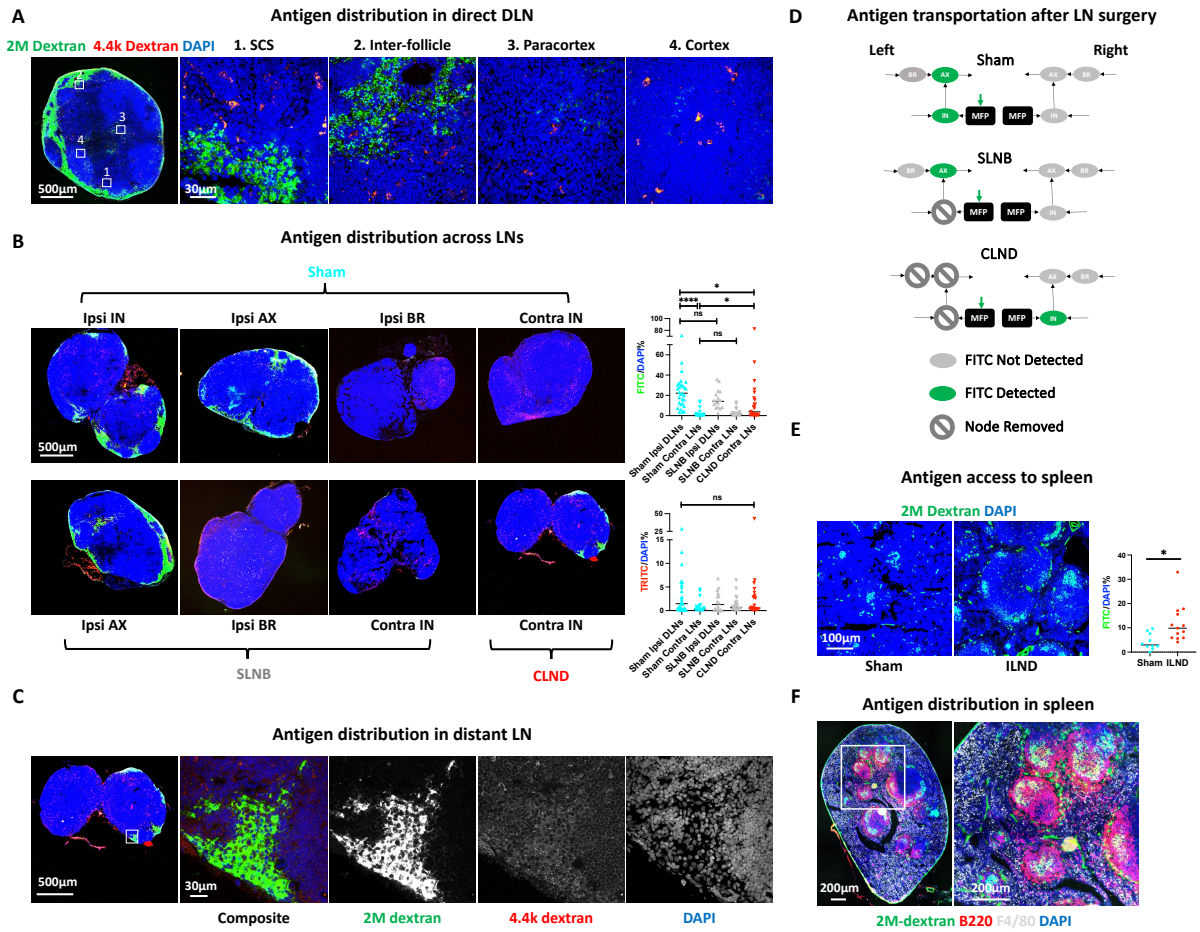

Figure 3. DLN dissection alters lymph drainage and promotes antigen access to distant lymphoid organs. FITC-conjugated 2 million Dalton (FITC-2MD) and TRITC-conjugated 4.4 kilodalton (TRITC-4.4kD) dextran were injected to the mammary fat pad of mice that underwent sham surgery, SLNB or CLND. (**A**) Representative immunofluorescence images of mouse with sham surgery demonstrate intranodal dextran distribution. (**B**) Dextran distribution in ipsilateral inguinal (IN), axillary (AX), brachial (BR) LNs as well as contralateral IN LNs in animals that underwent sham, SLNB or CLND. (**C**) Greater magnification image shows that large dextran molecules enter subcapsular sinus of contralateral IN LN in CLND mice, suggesting transport through lymphatic vessels. (**D**) Diagram shows lymph flow pattern in various surgery settings. (**E**) FITC-2MD dextran distribution in spleens from mice that underwent sham surgery or ipsilateral LN dissection (ILND). (**F**) Representative immunofluorescence images demonstrate

796 FITC-2MD dextran location in spleen from ILND mice relative to B cells (B220) and
797 macrophages (F4/80). In this figure, fluorescence signal quantification was calculated by the
798 occupied area, while DAPI was used to normalize LN area. Two tailed student t test (two
799 conditions) and one way ANOVA with Tukey post analysis (more than two conditions) were
800 used for statistical analysis. *$p<0.05$, **$p<0.01$, ****$p<0.0001$.
801

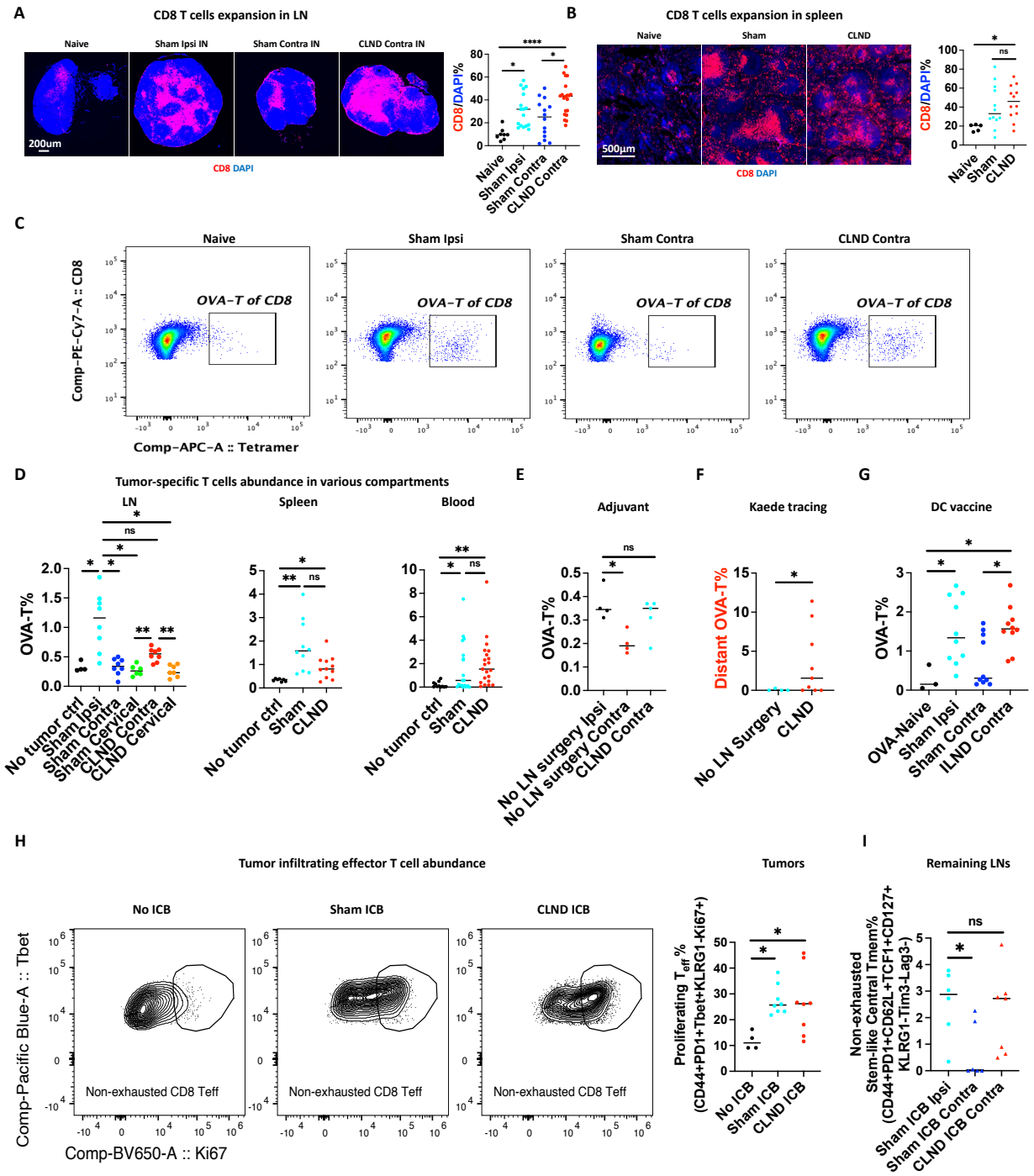

Figure 4. TDLN dissection stimulates immune responses in distant LNs. To assess the tumor-specific T cell response, B16F10 tumors overexpressing Ovabulmin$_{257-264}$ (OVA) were implanted to sham and CLND mice followed by anti-PD1 inhibition. (**A**) In ipsilateral and contralateral LNs as well as (**B**) spleens, CD8 T cell expansion is shown by immunofluorescence

807 images. (**C**) Additionally, OVA-specific CD8 T cells in ipsilateral, contralateral and cervical
808 LNs, spleens and blood were determined by tetramer staining using flow cytometry analysis. (**D**)
809 Abundance of OVA-specific CD8 T cells (CD8+, Tetramer+) is plotted for various LNs, blood
810 and spleens collected from sham and CLND mice; each dot represents data from a single mouse.
811 (**E**) OVA-specific CD8 T cell response in ipsilateral and contralateral LNs is shown in an
812 adjuvant setting where primary tumor resection was performed with or without CLND before
813 anti-PD1 inhibition. (**F**) Similar to **E**, Kaede mice bearing B16F10-OVA tumors were treated by
814 adjuvant anti-PD1 inhibition, followed by tumor rechallenge to primary site. Once recurrent
815 tumor formed, contralateral inguinal LNs were photoconverted prior to tissue harvesting for flow
816 analysis. Abundance of Kaede red+ tumor infiltrating OVA-specific CD8 T cells is plotted. (**G**)
817 To assess antigen-presenting cell-mediated T cell response after LN dissection, BMDCs were
818 pulsed with OVA and LPS for 1 day, and injected to the footpad of mice that underwent sham
819 surgery or ILND. OVA-specific CD8 T cells in ipsilateral and contralateral LNs are plotted. (**H**)
820 Abundance of tumor-infiltrating proliferating, non-exhausted CD8 effector T cell (CD44+,
821 PD1+, Tbet+, KLRG1-, Ki67+) in sham and CLND mice bearing B16F10 tumors treated by ICB
822 is shown. (**I**) Primary tumor resection was performed in sham and CLND mice treated by ICB,
823 and mice were rechallenged with B16F10 tumors subsequently. Abundance of non-exhausted
824 stem-like central memory CD8 T cells (CD44+, PD1+, CD62L+, TCF1+, CD127+, KLRG1-,
825 Tim3-, Lag3-) in remaining LNs is shown. In this figure, fluorescence signal quantification is
826 calculated by the occupied area, while DAPI is used to normalize. Two tailed student t test (two
827 conditions) and one way ANOVA with Tukey post analysis (more than two conditions) were
828 used for statistical analysis. *$p<0.05$, **$p<0.01$, ****$p<0.0001$.
829

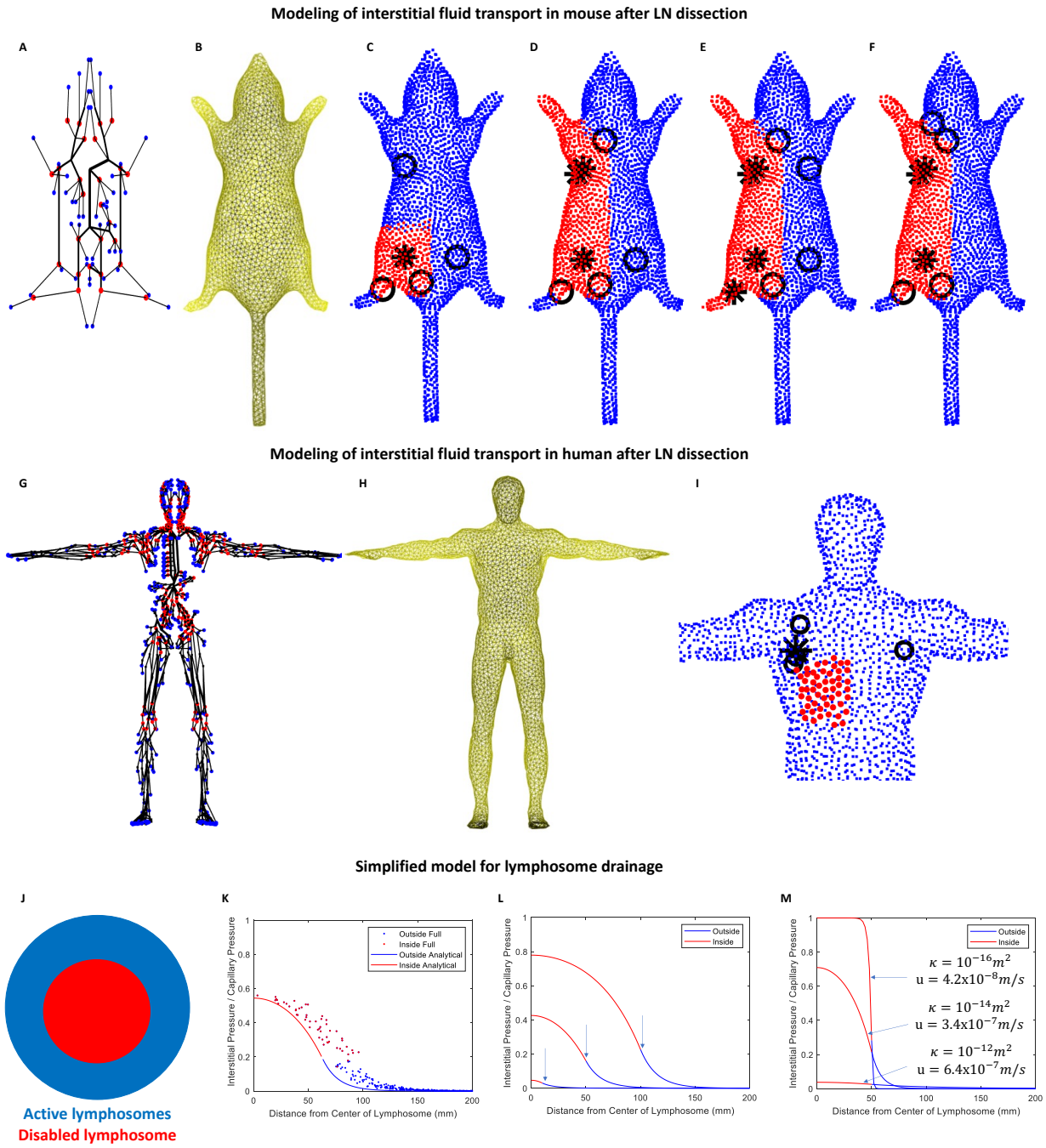

Figure 5. Mathematical modeling of antigen access to adjacent lymphosomes via dermal network after node dissection. (**A**) Mouse model with network of collecting lymphatic vessels (black), collecting points (blue) and lymph nodes (red). (**B**) Computational mesh for network of initial lymphatic vessels in the skin. (**C**-**F**) Drainage basins (red) with disabled nodes (black *), four most active compensatory nodes (black o) for (**C**) inguinal node resection, (**D**) inguinal and

836 axillary node resection, (**E**) popliteal, inguinal, axillary and brachial node resection, and (**F**)
837 inguinal and axillary node resection with severed midline model (intact **C**-**E**). (**G**) Human male
838 model with network of collecting lymphatic vessels (black), collecting points (blue) and lymph
839 nodes (red). (**H**) Computational mesh for network of initial lymphatic vessels in the skin. (**I**)
840 Drainage basin (red) with disabled axillary node (black *), four most active compensatory nodes
841 (black o). (**J**) Planar geometry for analytical model with a circular disabled lymphosome (red)
842 surrounded by tissue with active lymph clearance (blue). (**K**) Interstitial pressure inside and
843 outside of the disabled lymphosome from the full, 3D human model compared to an analytical
844 result for the planar geometry in (**J**) with the same surface area. (**L**) Dependence of interstitial
845 pressure on radius of disabled lymphosome (arrows) showing how small lymphosomes produce
846 little increase in interstitial pressure. (**M**) Dependence of interstitial pressure and fluid velocity u
847 at the periphery of the disabled lymphosome on tissue permeability (radius 50 mm) showing how
848 changes in tissue permeability can alter the interstitial pressure, but barely affects the rate of
849 fluid/antigen flow to compensatory lymphosomes (u).
850

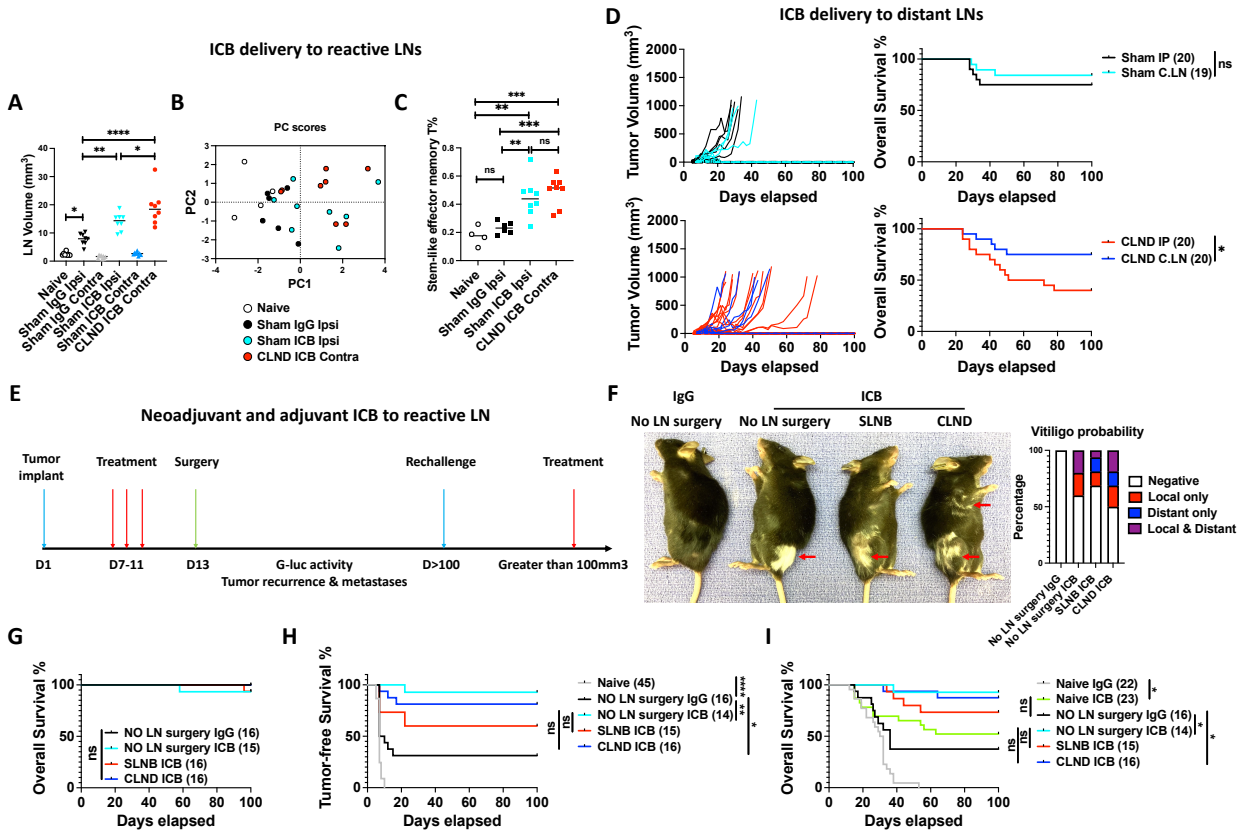

Figure 6. Distant LNs can be targeted to improve ICB response. Sham surgery or CLNB was performed on C57Bl6 mice (day -10) prior to orthotopic E0771 tumor implantation (day 1). IgG control or combination of anti-PD1 and anti-CTLA4 antibodies were intradermally delivered to ipsilateral TDLNs or contralateral LNs in sham and CLND conditions, respectively (day 7) for three doses at 5mg/kg. LNs exposed to treatment were harvested for flow cytometry analysis measuring CD45, TCR-beta, CD4, CD8, CD44, PD-1, TCF-1, CD39 and CD62L. Non-tumor bearing naïve mice are used as control. (**A**) LN Volume of naïve mice or mice treated by IgG or ICB combination is plotted. (**B**) Principle component analysis is performed on naïve or treatment-exposed LNs, using the abundance of antigen-experienced T cells (CD44+, PD-1+), memory T cells (CD44+, PD-1+, TCF1+), central memory T cells (CD44+, PD-1+, TCF1+, CD62L+), effector memory T cells (CD44+, PD-1+, TCF1+, CD62L-), stem-like effector memory T cells (CD44+, PD-1+, TCF1+, CD62L-, CD39-) and their CD4/CD8 subsets. (**C**) The

percentage of stem-like effector memory T cells to total T cells is plotted. (**D**) Using the same surgery, tumor implantation and treatment procedure, ICB was given intraperitoneally or intradermally to the lymphatic basin of contralateral inguinal LN (day 7) for three times at 5mg/kg in sham and CLND mice. Tumor volume (*left*) and overall survival (*right*) were plotted. (**E**) Timeline for neoadjuvant-adjuvant treatment and tumor rechallenge. (**F**) Representative images of vitiligo (arrows) that developed in mice after neoadjuvant treatment (*left*). Percentage of mice with local, distant or local & distant vitiligo across conditions (*right*). (**G**) Overall survival of mice treated by neoadjuvant ICB with various LN surgery status. (**H**) Tumor-free survival of mice previously treated by neoadjuvant ICB after tumor rechallenge. Naïve mice were used as control. (**I**) Overall survival of mice previously treated by neoadjuvant-adjuvant ICB after tumor rechallenge. Of note, only mice that developed tumors after rechallenge were given adjuvant treatment. In all studies, "(n)" indicates the number of mice used. One way ANOVA with Tukey post analysis (comparing more than two conditions) and Log-rank test with Bonferroni test (survival) were used for statistical analysis. *$p<0.05$, **$p<0.01$, ***$p<0.001$, ****$p<0.0001$.

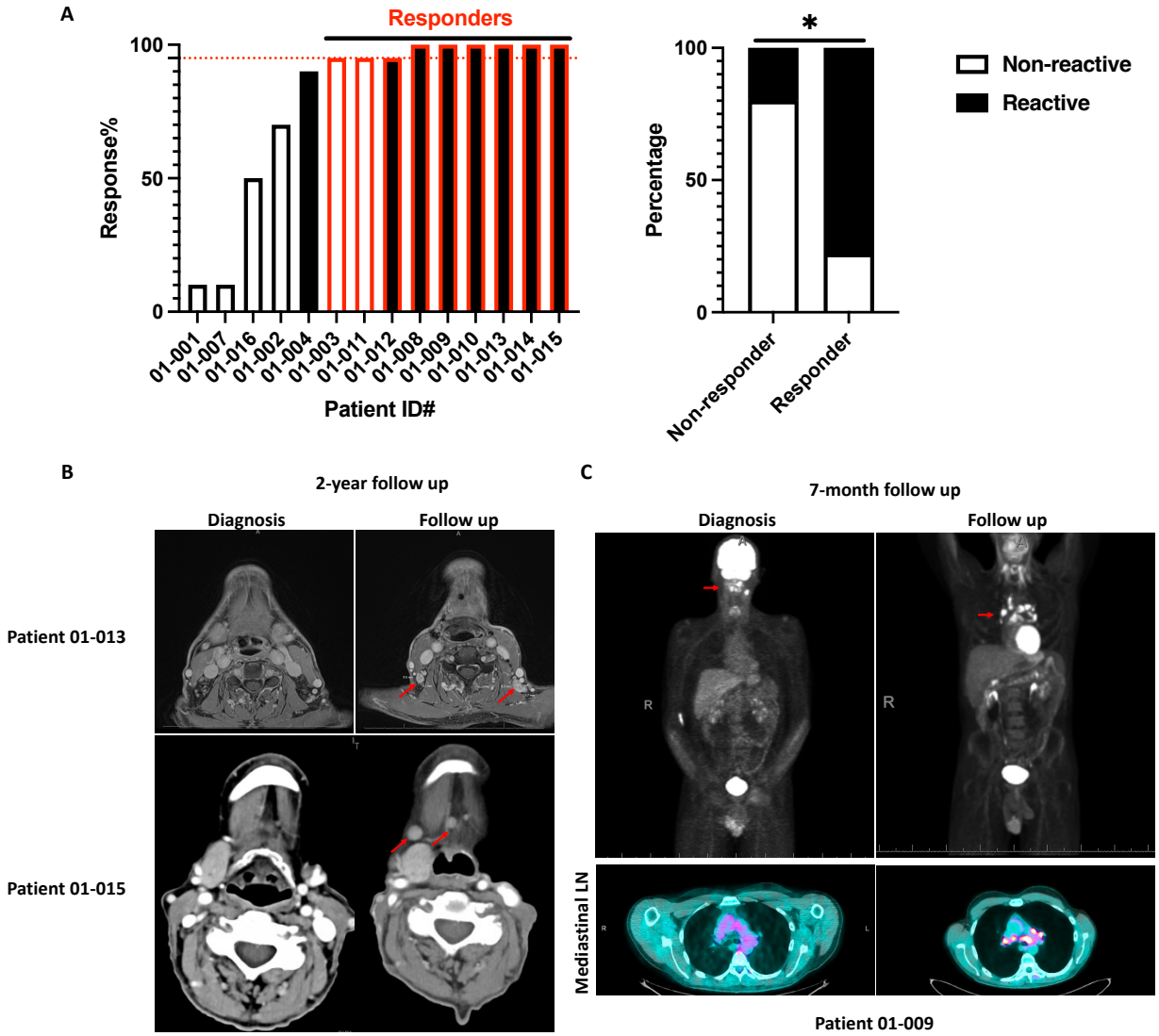

Figure 7. Distant LNs are inflamed after resection of tumor and related LNs in cancer patients. (**A**) *Left*, from phase I trial NCT03635164, response rate and reactive status of remaining LNs after neck dissection are shown. *Right*, percentage of patients that have enlarged or reactive LNs in more distal LN basins are plotted in non-responder and responder cohorts. Fisher's exact test 2x2 is used to evaluate statistical significance, *p<0.05. (**B**) CT images of patient 01-013's and 01-015's neck at diagnosis and 2-year post-surgery follow-up scan are demonstrated. Arrows indicate enlarged neck LNs (posterior cervical LNs in patient 01-013; submandibular and submental LNs in patient 01-015). (**C**) CT and PET images of patient 01-009

889 at diagnosis and 7-month post-surgery follow-up scan. Arrows indicate reactive cervical

890 (diagnosis) and apex mediastinal LNs (follow up).